SOME AERODYNAMIC CAVITY FLOWS IN FLIGHT PROPULSION SYSTEMS

William G. Cornell
Engineering Consultant - Aerodynamics
Jet Engine Department
General Electric Company

* * * * *

Some examples are given of the application of the Helmholtz-Kirchoff free-streamline theory of incompressible, potential flow, along with mixing calculations, to the practical estimation of separated gas flows occurring in several configurations taken from flight propulsion systems. Configurations considered are the perforated plate, the compressor-blade cascade, the vee-gutter flameholder, the target-type thrust reverser, the butterfly valve, and the perforated combustor liner. Results include cavity shape, drag force and total-pressure loss. The theoretical predictions are compared to experimental results in most cases and reasonable agreement is found in the areas wherein the theoretical assumptions are justifiable. The effects of compressibility and scale are discussed.

* * * * *

INTRODUCTION

In the development of modern air-breathing flight propulsion systems, powered by aircraft gas turbines and ramjets, certain internal aerodynamic problems arise due to the occurrence of separated flow, viz., streamlines which separate as a result of boundary layer action from the contours of immersed bodies or passage walls. Similar hydrodynamic problems arise in the fuel and propellant systems of liquid rocket engines.

In such separated flows, "dead water" regions are formed downstream of the points of separation of the fluid from the solid boundaries. Within the separated regions the fluid is more or less at rest relative to the moving fluid nearby. The separated regions may be styled as "aerodynamic cavities" in allusion to the true cavity flows in hydrodynamics, where gas filled cavities occur in similar liquid flows. In some cases, the separated flow is designed for (e.g., the separation regions of hot gas behind bluff-body flame holders in aircraft gas turbine and ramjet combustion systems). In other cases, the separated flow is not desired, but occurs under certain operating conditions (e.g., the separation regions of air behind stalled axial-compressor blades in aircraft gas turbines operating at off-design conditions).

In order to obtain optimum designs of the configurations in question, it is desired prior to model tests to predict the characteristics of the separated flow fields. The desired results are usually overall results rather than the complete details of the flow field (e.g., force on and geometry of separated region behind an immersed body, angular deflection and mass flow of a jet of gas, average total-pressure loss of gas flowing through a passage).

In cases where flow velocities are low (incompressible flow) and the flow configuration is made of or can be approximated by solid surfaces composed of linear elements, along with separated streamlines upon which static pressure is constant, and where the streamwise cavity length is long compared to configurational element size, the desired results are conveniently obtained by application of the free streamline method originated by Helmholtz (1) and Kirchoff (2) and perfected by Michell (3) and others. The method assumes an infinitely long cavity with steady, two-dimensional, body-force-free, potential flow of an incompressible, nonviscous fluid. As a result one obtains immersed-body force, separated region geometry, jet deflection, and mass flow. Mixing calculations then yield total-pressure loss in passage flow cases. With good approximation, certain three-dimensional flows can be treated by consideration of "equivalent" two-dimensional flows having the same "cross-sectional" areas for flow. In passage flow cases with higher flow velocities, the compressibility effect can be accounted for at least approximately by a compressible generalization of the mixing calculation, if theory or experiment is available for estimation of the geometry of the separated flow region. Scale effects (viscosity effects) may be neglected in cases where the separation points are fixed by sharp edges and where the fluid-friction forces in the average streamwise direction are negligible. In other cases, the qualitative nature of the scale effect may be estimated, as discussed elsewhere in the paper.

PHYSICAL CONCEPTS OF FREE STREAMLINE FLOWS

Early work (2) on free streamline flows included the case of a small sharp-edged orifice in an infinite plate and the case of a flat plate normal to an unbounded stream. In the former case, the theoretical contraction coefficient agreed well with experimental values obtained on both two-dimensional slits and round holes (4). In the latter case, the theoretical drag coefficients were found to be far lower than experimental values (5). This discouraging result impeded further practical applications of the method for many years.

At the root of the large difference between the two cases is the difference between two basic types of flow: (a) The relatively restricted flow of a jet through an opening, as in the case of the sharp-edged orifice, and (b) The relatively unrestricted flow of a free stream over an obstacle, as in the case of the flat plate. In the latter case, instability of the free boundary, small asymmetries, entrainment, etc., cause small motions in the cavity, the velocities of which cannot be neglected relative to the free stream velocity. In the former case, velocities likewise occur in the cavity, but are more nearly negligible relative to the large velocity of the jet. Thus, the fundamental assumption of a stagnant cavity is more justifiable in the case of the orifice than in the case of the plate and consequently there is better agreement between theory and experiment. This important point can be understood best by considering the two cases in question as limiting cases of the more general case shown in Fig. 1. The general case may be considered as a cascade consisting of an infinite number of sharp-edged flat plates of breadth* b, spaced apart by spacing t along a line normal

*See Nomenclature at end of text for definition and the units of all letter symbols.

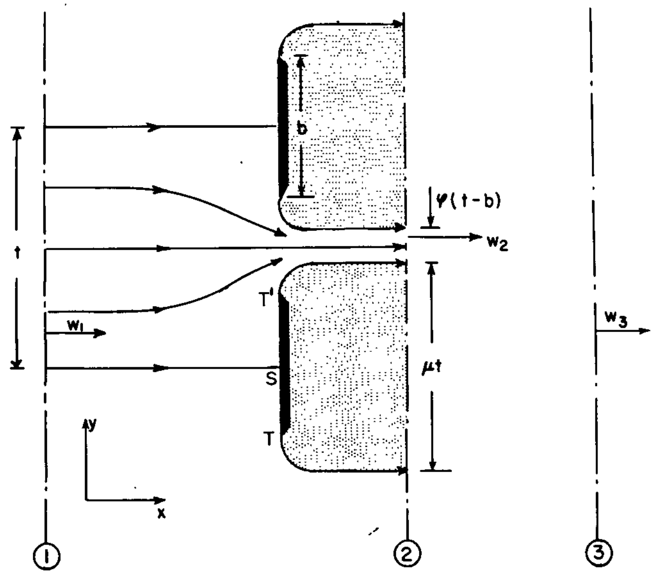

Fig. 1 - Model for flow in slat cascade

to the uniform parallel flow infinitely far upstream of the plates. The upstream flow at Section 1 in Fig. 1 has velocity w_1. Alternately, this case may be considered as an infinite number of sharp-edged orifices of opening $t - b$, spaced apart by spacing t. Separation regions or cavities extend infinitely far downstream and are enclosed by the free streamlines originating from the sharp edges T and T' of the solid boundaries. The static pressure is assumed to be constant at the downstream value on the free streamlines and within the cavity. Under the assumptions used, the fluid velocity is then constant on the free streamlines and discontinuously drops to zero in the cavity. Infinitely far downstream at Section 2, the cavities have width μt and are interspersed with jets of velocity w_2 and breadth $(1 - \mu)t$, or alternately, $\varphi(t - b)$, where φ is the "contraction coefficient" for the orifice case. The model is completed by visualization of a mixing region between Section 2 and Section 3, where a uniform parallel flow of velocity w_3 exists. The basic geometric parameter of the configuration is b/t. The case of the single plate is obtained by $b/t \to 0$, viz., $t \to \infty$. The case of the single orifice is obtained by $b/t \to \infty$, viz., $b \to \infty$. In the general case of $0 < b/t < \infty$, the jet velocity $w_2 > w_1$ by reason of continuity of flow, the ratio w_2/w_1 increasing as b/t increases. Thus, the validity of the stagnant cavity assumption increases as b/t increases, a result which is borne out by comparison of theory and test.

Therefore, internal flow configurations having cavities enclosed by jets having a velocity relatively high compared to the upstream velocity are particularly amenable to free streamline analysis. Since there is interest in other configurations (notably single bluff bodies) in which this is not the case, and since hydrodynamic cavities are frequently of finite length, numerous other theoretical methods based on various models of the flow have been developed in order to obtain better agreement between theory and experiment. Among these should be noted the model of Riabouchinsky (6) which employs a downstream "reflection image" of body and cavity, the model of Gilbarg and Rock (7) which has a finite cavity "ventilated" upstream into another

"Riemann sheet," and the model of Roshko (8) which uses an infinite cavity having linear boundaries far downstream. All of these models suffer from the requirement that either the drag coefficient or the pressure within the cavity be known from experiment in order that the flow model can be defined. A model proposed by Weinig (9) utilizes free streamlines which terminate in "winding points" in order to account somewhat for free boundary instability. Tulin (10) developed a "linearized" theory for relatively slender bodies. Any of these models can be used to improve the results of free streamline analysis of single bluff body or finite cavity cases, although analytical difficulties are sometimes large. The fact that such a large variety of models gives good results demonstrates the fact that the exact shape of the cavity does not affect the results too strongly.

The effects of compressibility and scale are discussed later in the paper.

ANALYTICAL METHODS FOR DETERMINATION OF FREE STREAMLINE FLOWS

The classical method for solution of free streamline problems grew* under the efforts of Helmholtz (1), Kirchoff (2), Michell (3), Planck (13), Christoffel (14), Schwarz (15), and Rayleigh (16) to the presently accepted method as delineated for example by Lamb (17) and especially well by Milne-Thomson (18). Thus, a flow field comprising linear solid boundaries and separated free streamlines is represented in the "physical" or $z = x + iy$ plane by a Laplacian net of streamlines (Ψ = constant) and potential lines (Φ = constant), described by the complex potential $W = \Phi + i\Psi$. The complex velocity† of flow is given by $\zeta = (u - iv)/U = dW/Udz$, where U is an arbitrary reference velocity. Thus, ζ may be used as a position variable to define a "hodograph" or ζ plane having the real coordinate u/U proportional to u, the x component of physical plane velocity, and the imaginary coordinate $-v/U$ proportional to the y component. Likewise, a "logarithmic hodograph" or $H = \ln(\zeta)$ plane may be defined, having the position variable $H = \ln\sqrt{(u^2 + v^2)/U^2} - i \tan^{-1}(v/u)$. Accordingly, the free streamlines in the z plane may be conformally transformed to circles about the origin in the ζ plane and lines parallel to the imaginary axis in the H plane. Likewise, the linear solid boundaries transform to rays from the origin in the ζ plane and lines parallel to the real axis in the H plane. Thus, the physical flow configuration in the z plane may be studied in terms of the relatively simpler configurations of circular arcs and rays in the ζ plane and of straight lines in the H plane.

The physical problem involves the determination of the complex potential $W(z)$, the complex velocity $\zeta(z)$ and finally the static pressure p from the Bernoulli relation $p + (1/2)\rho(u^2 + v^2)$ = constant. The relation $W(z)$ is obtained indirectly through an auxiliary variable Z so defined that the Z plane is a half-plane on the real axis of which is mapped the polygonal boundary of the flow field in the H plane, by means of the Schwarz-Christoffel transformation function. Also mapped on the Z plane is the (rectangular) polygonal boundary of the flow field in the $W = \Phi + i\Psi$ plane. Thus, the relations $H(Z)$ and $W(Z)$ are obtainable from the mappings. Then, the relation $z(Z)$ is obtainable by integration as $z(Z) = (1/U)\int e^{-H(Z)}[dW(Z)/dZ]dZ$. Finally, having $H(Z)$, $W(Z)$, and $z(Z)$, there is obtained, at least implicitly, $W(z)$ and, therefore, $\zeta(z)$ and $p(z)$.

The "classical" method just described can be used in any free streamline problem, although there is no guarantee that a closed-form solution can be obtained, since

*See McNown (11) and Birkhoff (12) for interesting historical discussions of the method and its practical application.
†The convention $dW/dz = +u - iv$ is used herein.

integrals sometimes occur which cannot be evaluated analytically. A less general but simpler method can be used in some cases, viz., when the flow field $W(\zeta)$ in the hodograph plane can be synthesized by physical reasoning. Then $W(\zeta)$ is obtained by integration of $z(\zeta) = (1/U) \int \zeta^{-1}(dW/d\zeta)d\zeta$.

EXAMPLE OF THE SLAT CASCADE

As an example of the sort of application of the free streamline method considered herein, the slat cascade may be treated. The two-dimensional model is shown in Fig. 1, characterized by the blocked area ratio b/t. Equivalent configurations of practical interest are the three-dimensional (same blocked area ratio) sharp-edged orifice plate, the sharp-edged orifice symmetrically placed in a channel, the perforated plate strainer, and the ribbon screen. It is desired to predict the total-pressure loss, the drag force on the solid elements, and the flow through the cascade. The solution may be obtained as a special case of the solution for the stalled flat plate cascade (19) or, for illustrative purposes, maybe developed as follows, utilizing the alternative physical synthesis approach discussed above. Let the $z = x + iy$ plane contain the slat cascade with the origin taken at the center of one of the infinitesimally thin plates. Under the previously stated assumptions of the free streamline theory there exists a complex potential function $W = \Phi + i\Psi$, where Φ and Ψ are respectively potential and stream functions. The nondimensional complex velocity of the flow is taken as $\zeta = (u - iv)/w_2$ where u and v are respectively the x and y components of z plane velocity and where w_2 is the uniform velocity of the jets at $x = +\infty$. Since $\zeta = dW/w_2dz$ is an analytic function of z, assuming W to be likewise, the z plane may be conformally transformed to or mapped upon the ζ plane, (nondimensional conjugate hodograph plane) yielding another Laplacian net of Φ and Ψ lines, which may be visualized as a physically fictitious potential flow field in itself. A point-to-point reciprocal correspondence then exists between the planes of z and ζ, defined by the transformation function $z = z(\zeta)$, as yet unknown.

The flow field in the ζ plane is shown in Fig. 2, and may be physically deduced to be so as follows: The flow in each strip of width t in the z plane maps into the

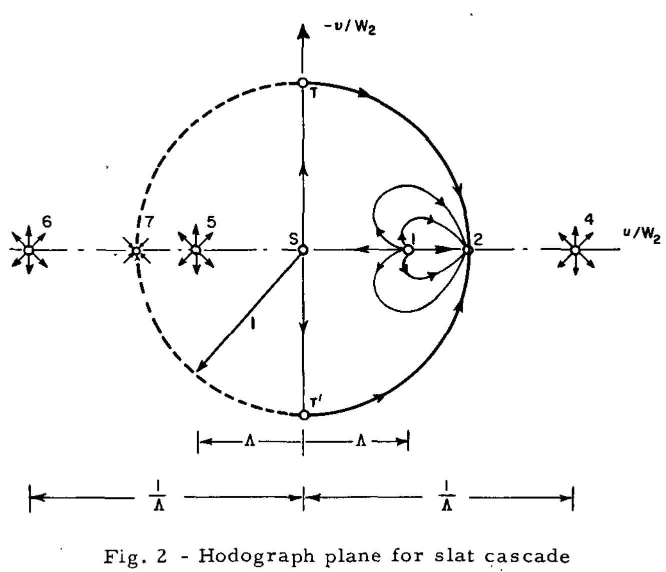

Fig. 2 - Hodograph plane for slat cascade

unit semicircle in the ζ plane. All streamlines (total volume of flow = $w_1 t$) emanate from the point $\zeta_1 = \Lambda$, the transformed image of the line $z_1 = -\infty$, and terminate in the point $\zeta_2 = +1$, the transformed image of the line $z_2 = +\infty$. The plate surfaces TT' map into the imaginary axis. The free streamlines T2 and T'2 map into the unit semicircle. All streamlines of the flow in the z-plane strip map into streamlines contained within the ζ plane semicircle. The mapping is repetitive in that each z-plane strip maps into the same ζ-plane semicircle.

The nature of the flow at ζ_1 is that of a source of strength (volume flow) $w_1 t$, while at ζ_2 there must exist a double sink of strength $2w_1 t$. This follows from consideration of the symmetric nature of the ζ_1 flow and from the requirement that the imaginary axis and the unit semicircle be streamlines of the ζ-plane flow. The latter requirement further demands the existence of the sources (strength $w_1 t$) at ζ_4, ζ_5, and ζ_6 and the double sink (strength $2w_1 t$) at ζ_7. The "reflection singularities" added in the ζ plane are without (or on) the boundary of the unit semicircle and hence do not imply nonphysical image singularities in the z-plane flow. Finally, all required boundary conditions in the z-plane and ζ-plane flows are satisfied and the ζ-plane flow field is given by the complex potential due to the six singularities as

$$W(\zeta) = (w_1 t/2\pi)[\ln(\zeta^2 - \Lambda^2) + \ln(\zeta^2 - 1/\Lambda^2) - 2\ln(\zeta^2 - 1)] . \tag{1}$$

The complex velocity of the ζ-plane flow field is then given by

$$dW/d\zeta = (w_1 t/2\pi)[2\zeta/(\zeta^2 - \Lambda^2) + 2\zeta/(\zeta^2 - 1/\Lambda^2) - 4\zeta/(\zeta^2 - 1)]. \tag{2}$$

The derivative of the transformation function $z(\zeta)$ is then given by

$$\begin{aligned} dz/d\zeta &= \frac{dW/d\zeta}{dW/dz} = \frac{dW/d\zeta}{w_2\zeta} \\ &= (w_1 t/2\pi w_2\zeta)[2\zeta/(\zeta^2 - \Lambda^2) + 2\zeta/(\zeta^2 - 1/\Lambda^2) - 4\zeta/(\zeta^2 - 1)] \end{aligned} \tag{3}$$

which equation may be integrated to yield

$$z = (\Lambda t/2\pi)\left\{\frac{1}{\Lambda}\ln\frac{\zeta - \Lambda}{\zeta + \Lambda} + \Lambda\ln\frac{\Lambda\zeta - 1}{\Lambda\zeta + 1} - 2\ln\frac{\zeta - 1}{\zeta + 1}\right\} + C_1 \tag{4}$$

where C_1 is an arbitrary constant of integration. Equation (4) is the transformation function $z(\zeta)$ linking points in the z and ζ planes.

The ζ-plane parameter Λ may now be evaluated from use of the physical condition that the plate breadth b is given by the relation

$$b = (1/i)(z_{T'} - z_T). \tag{5}$$

Substituting (4) in (5) with $\zeta_{T'} = -i$ and $\zeta_T = +i$, yields the relation

$$b/t = 1 - \Lambda - (2/\pi)(1 - \Lambda^2)\,\mathrm{tg}^{-1}(\Lambda) \tag{6}$$

which gives the parameter $\Lambda = w_1/w_2$ implicitly in terms of the blockage b/t. Thus, the ζ plane is completely determined for a chosen z-plane geometry b/t, and the z-plane complex velocity $u - iv = w_2\zeta$ can be determined at any point. In particular, at the point ζ_2, the complex velocity is $u_2 = w_2 = w_1/\Lambda$.

Continuity of flow in the z-plane requires that

$$w_2(1 - \mu)t = w_1 t \tag{7}$$

so that

$$\mu = 1 - \Lambda \tag{8}$$

is obtained for the cavity width parameter and $\mu = \mu(b/t)$ is obtained from (6) and (8).

The result may be expressed in terms of the contraction coefficient defined geometrically by

$$\varphi = (1 - \mu)/(1 - b/t) \tag{9}$$

which yields $\varphi = \varphi(b/t)$ from (6), (8), and (9).

The drag force per unit span D on one of the slats may be expressed as a non-dimensional drag coefficient $C_D = D/(1/2)\rho w_1^2 b$ as

$$C_D = (1 - \Lambda)^2 (t/b)/\Lambda^2 \tag{10}$$

from application of the momentum principle to one strip of fluid of breadth t and from consideration of the Bernoulli relation for the lossfree flow between Sections 1 and 2. Then, (6) and (10) yield $C_D(b/t)$.

The total-pressure loss $\Delta p_T = p_{T1} - p_{T3}$ may be calculated under the assumption of constant momentum mixing of the jets and cavities at Section 2 to yield a uniform stream of velocity $w_3 = w_1$ at Section 3. Thus, applying the momentum principle and the continuity principle to the fluid between Sections 2 and 3 and noting that $p_{T2} = p_{T1}$ as assumed, it follows that the total-pressure loss coefficient $\lambda = \Delta p_T/(1/2)\rho w_1^2$ is given by

$$\lambda = (1 - \Lambda)^2/\Lambda^2 \tag{11}$$

so that (6) and (11) yield $\lambda(b/t)$.

Plots of velocity ratio Λ, contraction coefficient φ, drag coefficient C_D and loss coefficient λ against blockage b/t are shown in Figs. 3a-3d, compared to two- and three-dimensional (same blockage) experimental data on various configurations. Figure 3a shows the theoretical prediction for $\Lambda(b/t)$ compared to experimental data of Betz and Petersohn (20) for the cases of water discharging into air (circled points) and air into air (x points). It will be noted that the former tests agree most closely with theory. Figure 3b compares the theoretical $\varphi(b/t)$ with pipe orifice water tests of Weisbach (21) and axisymmetric nozzle air tests of Grey and Wilsted (22). The two-dimensional theory is compared to the three-dimensional data at the same blockage b/t. Figure 3c shows the theoretical prediction for

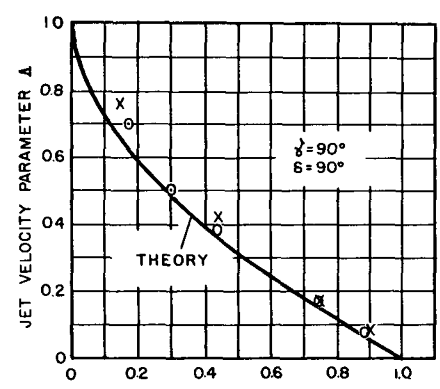

Fig. 3a - Comparison of theory and experiment for jet velocity parameter of slat cascade

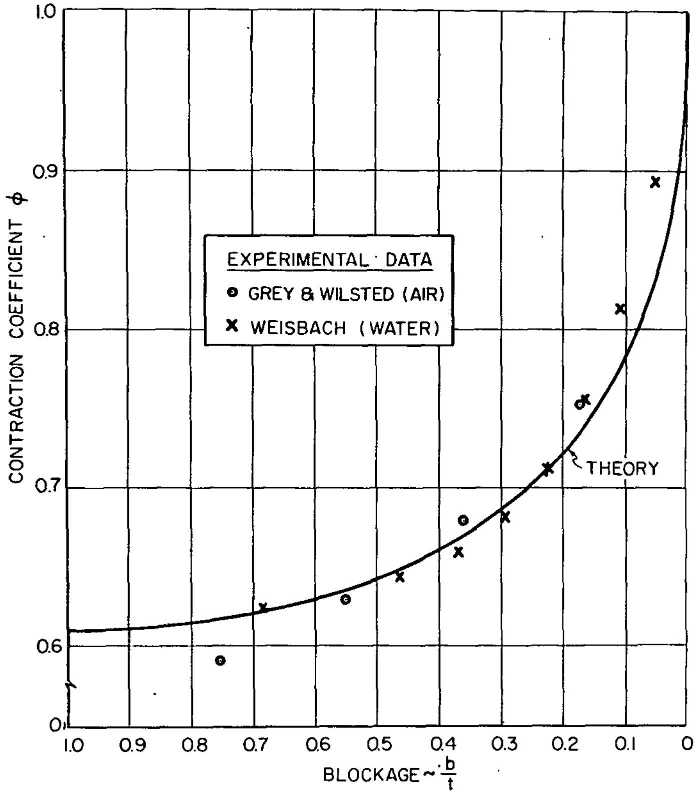

Fig. 3b - Comparison of theory and experiment for contraction coefficient of slat cascade

$C_D(w_1/w_2)^2$, or drag coefficient based on jet velocity head, compared to air tests of Langer (23), who measured slat forces with a two-component balance. Figure 3d compares the theoretical $\lambda(b/t)$ to the test results of various investigators (24) on perforated plate strainers, ribbon screens, and strip screens. The test results agree reasonably well with the theory, especially at high solidity or blockage b/t, for which cases the stagnant cavity assumption is most valid. Generally, experimental values of $\mu = 1 - \Lambda$, C_D, and λ are less than theory predicts, undoubtedly due in part to the lack of perfect sharpness of the experimental plate edges.

THE STALLED CASCADE OF ARBITRARY STAGGER

In off-design performance analysis of axial-flow compressors for aircraft gas turbines, it is important to be able to predict the performance of blade rows operating in stalled condition. A simple model (19) of a blade row is the two-dimensional cascade of infinitesimally thin flat plates shown in Fig. 4 and characterized geometrically by solidity l/t and stagger γ. The configuration is a generalization of that of the slat cascade ($\gamma = 90°$, $\beta_1 = 0°$) previously discussed and may be analyzed by a similar method.

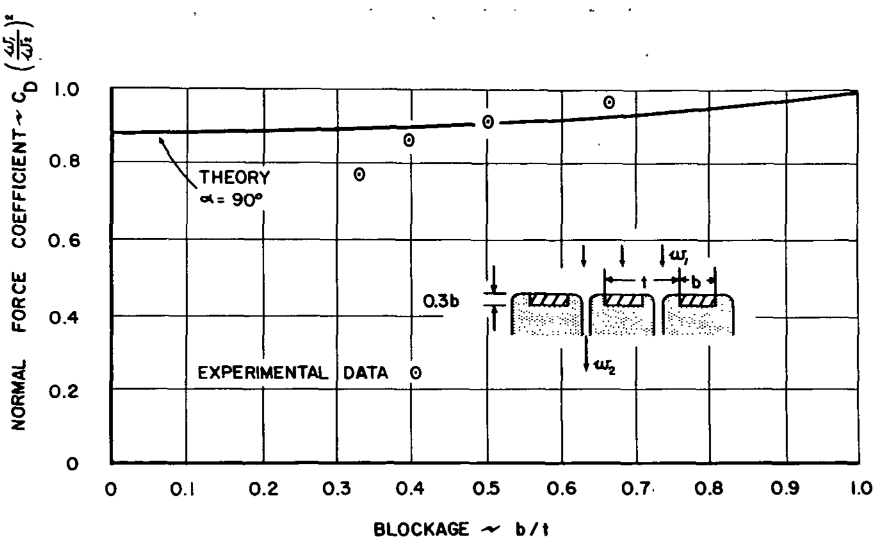

Fig. 3c - Comparison of theory and experiment for normal-force coefficient of slat cascade

In the generalized case, the flow is complicated by the fact that the cascade causes a deflection $\theta = \beta_1 - \beta_2$ of the jets, while the mixing of jets and cavities causes a further deflection, to yield an overall deflection $\epsilon = \beta_1 - \beta_3$. The situation is conveniently visualized in terms of the conventional "velocity triangle" of the cascade, as shown in Fig. 5. It is noted that w_1 and w_3 have equal x components (normal to cascade axis) as a result of continuity of flow, while w_2 and w_3 have equal y components (along cascade axis) as a result of momentum considerations. The conventional "vector mean velocity" w_∞ and its inclination β_∞ are defined such that

$$2 \tan \beta_\infty = \tan \beta_1 + \tan \beta_3 \tag{12a}$$

$$w_\infty/w_1 = \cos \beta_1/\cos \beta_\infty \,. \tag{12b}$$

The free streamline analysis of Betz and Petersohn (20) yields the jet velocity parameter $\Lambda = w_1/w_2$ and the jet flow angle β_2 as functions of cascade geometry $1/t$ and γ and of angle of attack $\delta = \beta_1 - \gamma$. The cavity width parameter μ then follows from consideration of continuity of flow as

$$\mu = 1 - \Lambda \cos \beta_1/\cos \beta_2 \,. \tag{13}$$

Analysis of the mixing of jets and cavities (19) then yields the overall cascade performance. Thus, the final velocity w_3 and its inclination β_3 are obtained from continuity and momentum consideration as

$$w_3/w_2 = \sin \beta_2[1 + (1 - \mu)^2/\tan^2 \beta_2]^{1/2} \tag{14a}$$

$$\tan \beta_3 = \tan \beta_2/(1 - \mu) \,. \tag{14b}$$

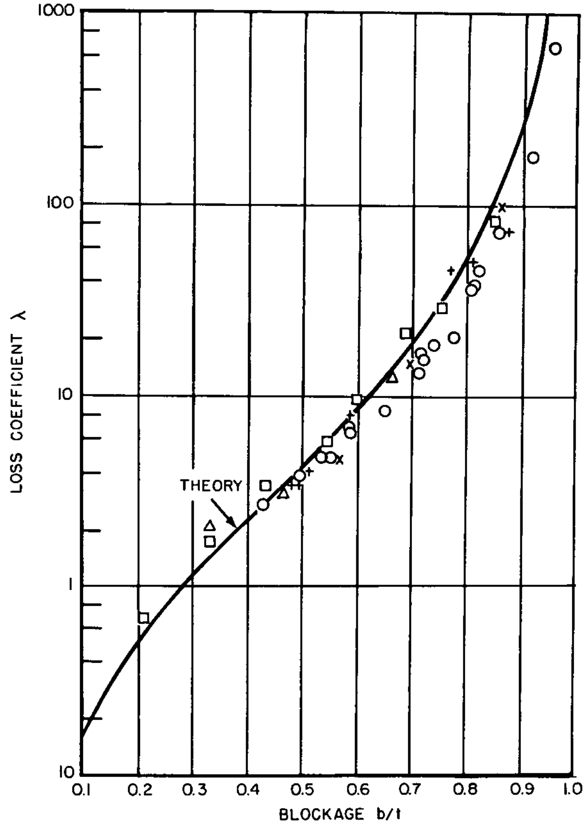

Fig. 3d - Comparison of theory and experiment for total-pressure loss coefficient of slat cascade

The vector mean velocity w_∞ and its inclination β_∞ are then obtained from (12) and the overall changes in static and total pressure are obtained from continuity and momentum considerations as

$$(p_3 - p_1)/(1/2)\rho w_\infty^2 = \cos^2\beta_\infty\left\{[2\mu/(1-\mu)] - \sec^2\beta_1(1-\Lambda^2)/\Lambda^2\right\} \tag{15a}$$

$$(p_{T1} - p_{T3})/(1/2)\rho w_\infty^2 = \cos^2\beta_\infty \mu^2/(1-\mu)^2 . \tag{15b}$$

The force N on each plate is normal to the plate and may be expressed in terms of a normal force coefficient $C_{N\infty} = N/(1/2)\rho w_\infty^2$, referred to w_∞. Then, conventionally, the total plate force may be resolved into the lift L and drag D forces, respectively normal and parallel to w_∞. Then, the lift and drag coefficients are given by

$$C_{L\infty} = L/(1/2)\rho w_\infty^2 l = C_{N\infty} \cos(\beta_\infty - \gamma) \tag{16a}$$

$$C_{D\infty} = D/(1/2)\rho w_\infty^2 l = C_{N\infty} \sin(\beta_\infty - \gamma) . \tag{16b}$$

The normal force coefficient $C_{N\infty}$ is obtained from momentum considerations as

$$C_{N\infty} = (\cos^2\beta_\infty/\cos^2\beta_1)(t/l) \Big\{- \sin\gamma\,[(1 - \Lambda^2)/\Lambda^2] + 2\cos\beta_1[\sin(\beta_1 - \gamma) - (1/\Lambda)\sin(\beta_2 - \gamma)]\Big\} . \quad (17)$$

Then, (16) and (17) may be used to obtain $C_{L\infty}$ and $C_{D\infty}$.

Typical theoretical results (19) are shown in Figs. 6a-6c for the case of the stagger $\gamma = 30°$ and the angle of attack $\delta > 0$. Companion results for $\delta < 0$ (turbine case) are given in Ref. 19. Figure 6a shows the relation among jet velocity ratio Λ, jet turning angle θ, solidity l/t, and angle of attack δ. Figure 6b shows the relation among overall turning ϵ, loss coefficient λ, l/t, and δ. Figure 6c shows the "polar diagram" where lift coefficient $C_{L\infty} = C_L(w_1/w_\infty)^2$ is plotted as a function of drag coefficient

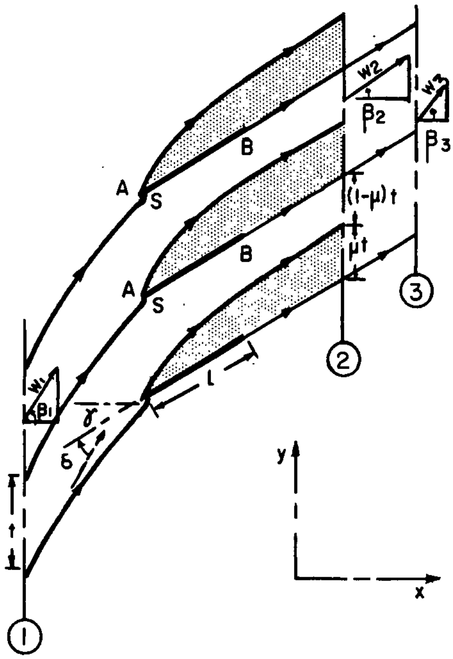

Fig. 4 - Model for flow in stalled cascade of stagger γ

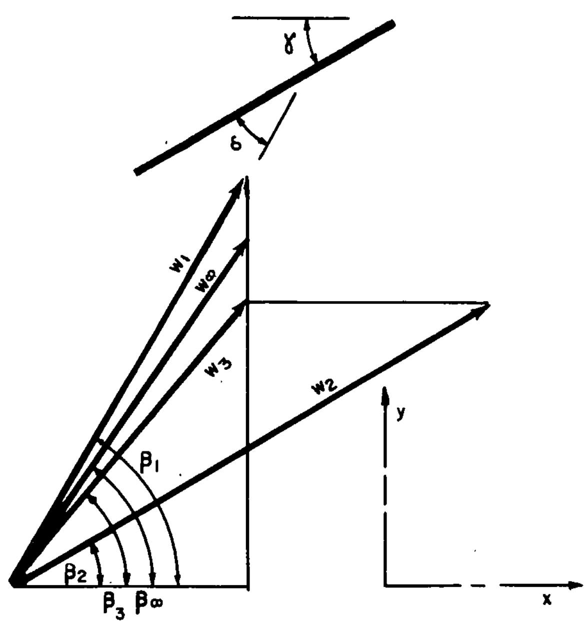

Fig. 5 - Velocity triangle for stalled cascade

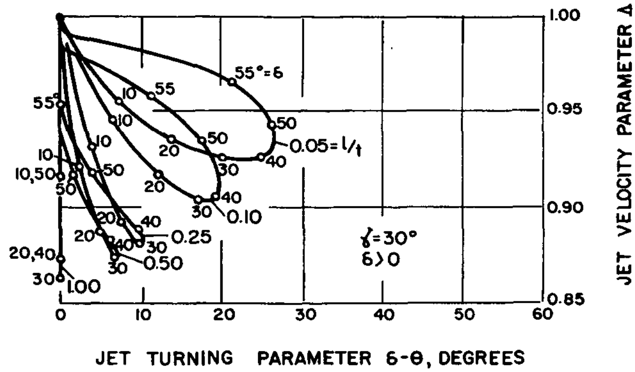

Fig. 6a - Theoretical jet turning angle and jet velocity parameter of stalled cascade

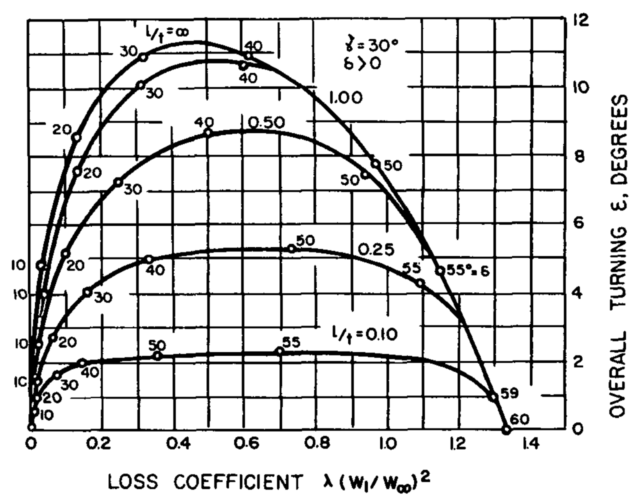

Fig. 6b - Theoretical overall turning angle of stalled cascade

$C_{D\infty} = C_D(w_1/w_\infty)^2$ for various l/t and δ. Figures 7a and 7b show comparisons of the theoretical results with experimental results of various investigators. Figure 7a compares the theoretical predictions of Λ and θ with experimental air test data of Betz and Petersohn (20) for $l/t = 1.2$, inlet angle $\beta_1 = 0$, and various stagger γ. Figure 7b shows theoretical normal-force coefficient $C_N(w_1/w_2)^2$ for various solidity l/t, and several values of angle of attack δ and stagger $\gamma = 90°$, compared to air test results of Langer (23). Experimental values of Λ and θ exceed theoretical predictions, the discrepancy undoubtedly being due in part to the lack of perfect edge sharpness. The low values of normal-force coefficient at low incidence probably imply the lack of fully developed stall. The force coefficient comparison shows improvement in agreement between theory and test as solidity increases, a trend shown by other experimental data on Λ and θ (19).

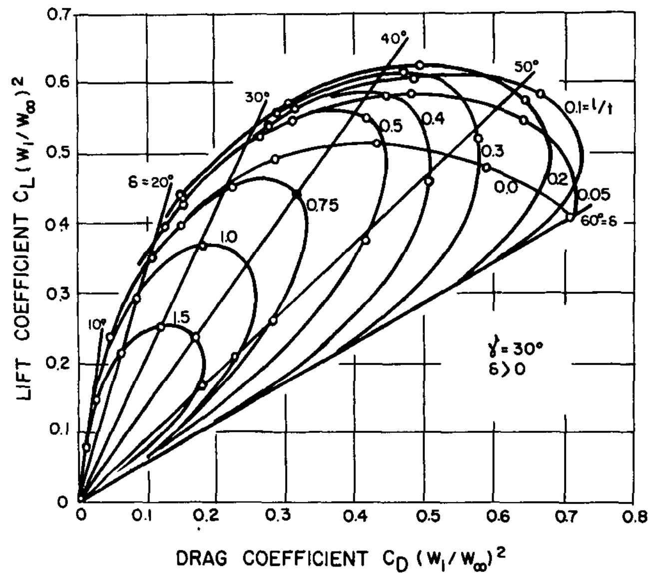

Fig. 6c - Theoretical lift-drag polar of stalled cascade

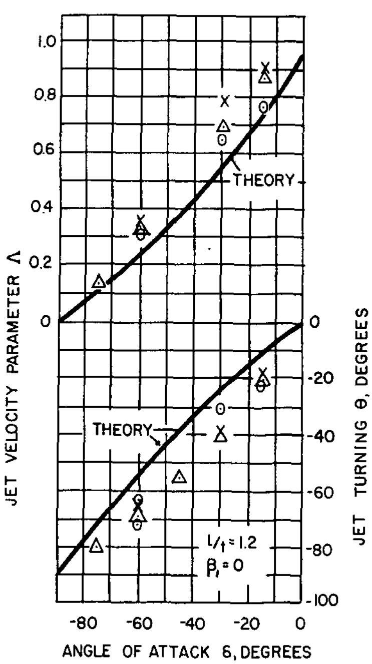

Fig. 7a - Comparison of theory and experiment for jet velocity parameter and jet turning angle of stalled cascade of 1.2 solidity and zero inlet angle

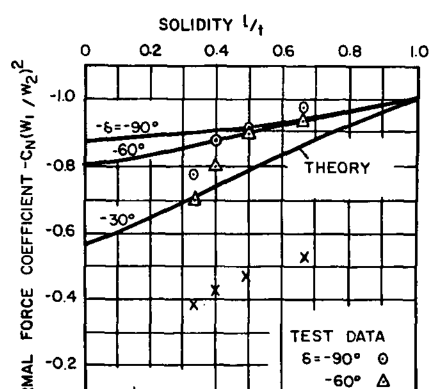

Fig. 7b - Comparison of theory and experiment for normal-force coefficient of stalled cascade of 90° stagger

THE VEE-GUTTER FLAMEHOLDER

In afterburners of aircraft gas turbine power plants and in ramjet combustors, various bluff bodies are used as flameholders, the downstream cavities being used to stabilize combustion. A typical configuration is composed of concentric rings of vee cross-section. A simple model (25) is the two-dimensional vee-gutter cascade shown in Fig. 8. The configuration may be considered to be a generalization of the slat cascade ($\alpha = 90°$), with the additional geometrical variable of gutter-included half-angle α. The desired results are again the cavity width parameter μ, the drag coefficient C_D and the total-pressure loss coefficient λ for a chosen cascade geometry given by blockage b/t and half-angle α.

The configuration of the vee-gutters and cavities is aerodynamically equivalent, under the assumptions made, to the two-dimensional contraction of wall angle α and area ratio $1 - b/t$. The contraction was analyzed by von Mises (26), utilizing the classical method, in order to obtain the contraction coefficient $\varphi = (1 - \mu)/(1 - b/t)$ as a function of b/t and α, a result useful in the prediction of flow through conical exhaust nozzles (same area ratio) of turbojet engines. The theoretical results of von Mises (26) are shown in Fig. 9 in terms of μ as a function of b/t and α.

Then, as in the case of the slat cascade, drag coefficient C_D and loss coefficient λ are calculated (25) as functions of b/t and α by application of the continuity and momentum principles. The theoretical results are shown in Figs. 10a and 10b. In Figs. 11a-11c, the theoretical results are compared (25) to experimental results of various investigators. Figure 11a compares theoretical values of wake width to pitch ratio μ for various half-angle α and blockage b/t to experimental results of Grey and Wilsted (22) for air tests of conical nozzles. The experimentally determined contraction coefficients are expressed in terms of equivalent values of μ for the comparison. Figure 11b shows theoretical drag coefficient $C_D(w_1/w_2)^2$ for $\alpha = 140.5°$ and various b/t compared to experimental data of Langer (23) from air tests. Figure 11c compares the theoretical prediction for loss coefficient λ for $\alpha = 45°$ and various b/t with air and combustion gas test results of Noreen (27) on two-dimensional single-gutter flameholder models. In general, theory and experiment compare best at high blockage b/t.

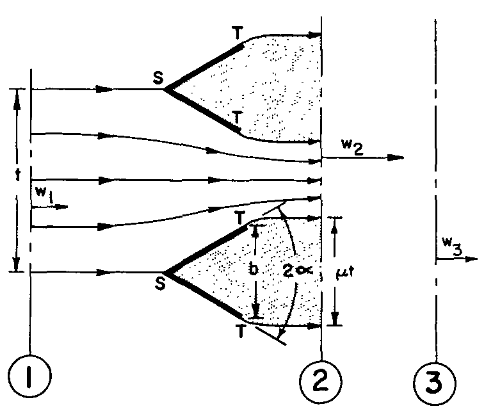

Fig. 8 - Model for flow in vee-gutter cascade

THE TARGET-TYPE THRUST REVERSER

In order to slow down jet aircraft upon landing, without decreasing engine rotative speed so much that large engine acceleration times would be required should landing plans be abandoned, a variety of jet thrust spoilers and reversers have been investigated. One type of jet thrust reverser is the target type, in which an obstacle of concave form on the upstream face is inserted across the jet in order to deflect the jet upstream, thereby providing some reverse or negative thrust. For design purposes, it is desired to obtain the shape of and velocity in the deflected jet as a function of target geometry, so that effectiveness of thrust reversal may be studied.

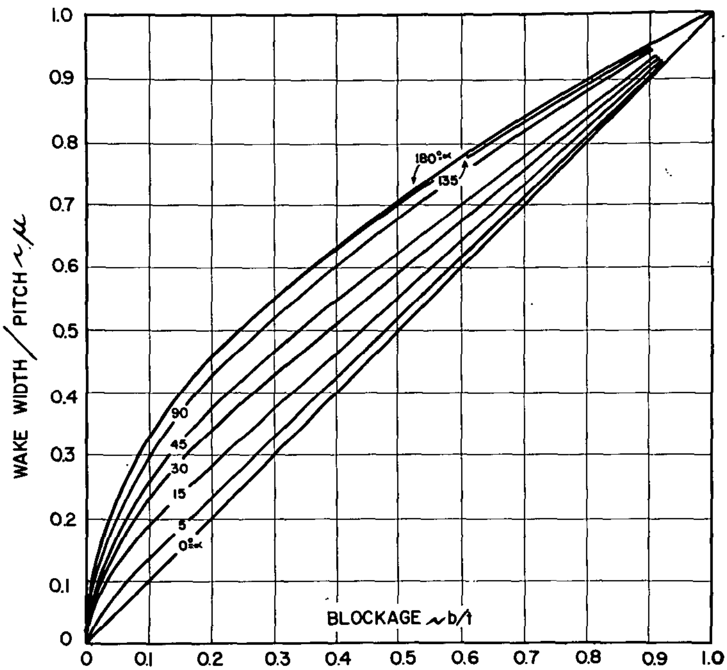

Fig. 9 - Theoretical wake width to pitch ratio of vee-gutter cascade

Considering a cylindrical thrust reverser of internal diameter D and axial length c, positioned symmetrically across a jet of diameter d, the equivalent two-dimensional configuration is shown in Fig. 12. The model reverser has axial length c and breadth b, the upstream jet breadth being a, where $c/a = c/d$ and $b/a = (D/d)^2$ define the equivalence of the two- and three-dimensional configurations. The initial jet of breadth a and velocity w_1 splits into two symmetrical jets of width a/2 and velocity w_1, since the jets are bounded by the free streamlines along which the velocity is taken as constant. The desired result is the jet deflection angle ν as a function of target and jet geometry b/a and c/a. Sarpkaya (28) has analyzed the configuration by the classical method in order to study the flow in water turbine "scoop" buckets. The theoretical results are shown in Fig. 13, compared to three-dimensional test data of Siao and Hubbard (29) and De Haven (28) taken with water jets in air. The check between theory and test is best at low b/a and low c/a, suggesting that frictional effects may be responsible for the lack of better agreement.

A similar analysis may be made of a conical target of internal diameter D and included angle $2(\pi - \alpha)$ positioned symmetrically across a jet of diameter d. The equivalent two-dimensional configuration, shown in Fig. 14, has breadth b and included angle $2(\pi - \alpha)$, the jet breadth being a, where $b/a = (D/d)^2$ defines the equivalence. The desired result is jet deflection angle ν as a function of target and jet geometry b/a and α. Siao and Hubbard (29) analyzed the model configuration by the classical method in order to study water turbine bucket flows. Their theoretical results are shown in Fig. 15, compared with results of their three-dimensional experiments on water jets in air. Measured deflection angles are lower than predicted and increasingly so at larger b/a, presumably due mostly to the effect of friction and possibly also to the lack of perfect sharpness of test plate edges.

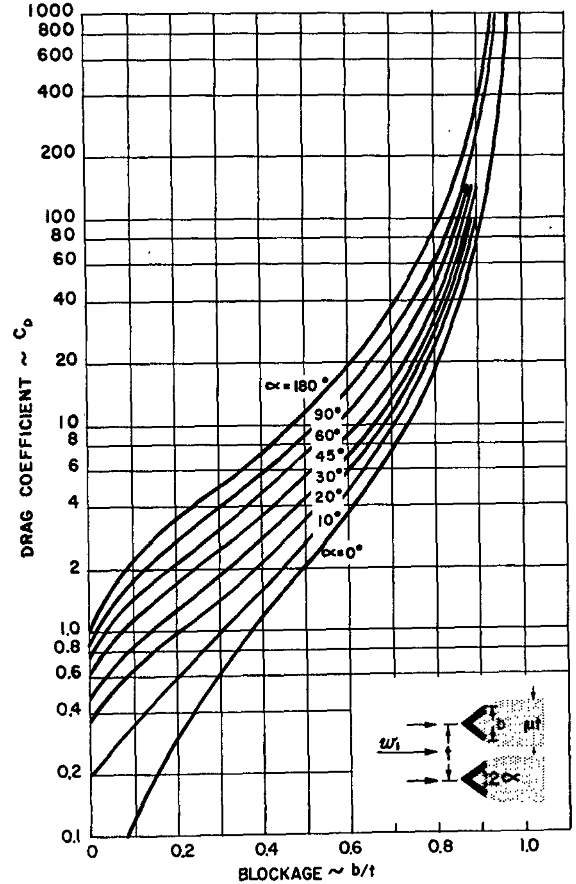

Fig. 10a - Theoretical drag coefficient of vee-gutter cascade

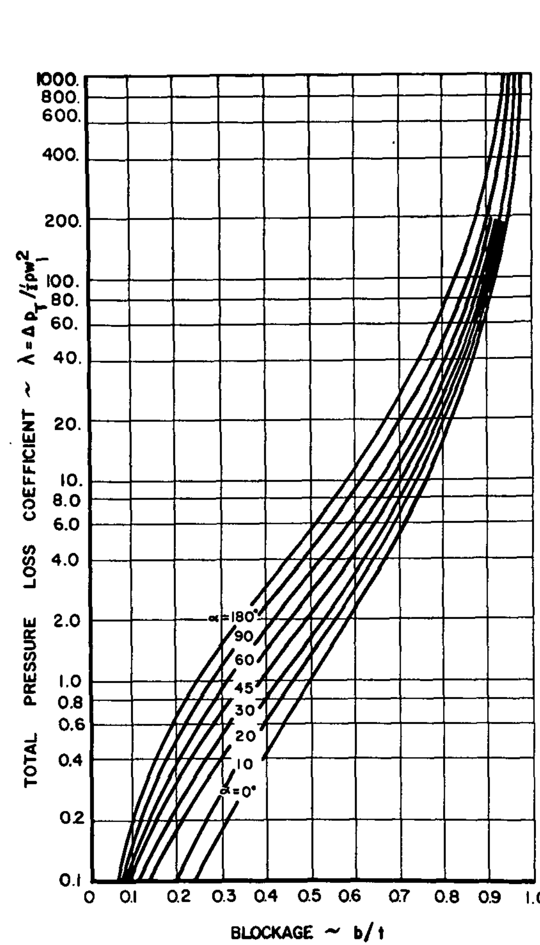

Fig. 10b - Theoretical total-pressure loss coefficient of vee-gutter cascade

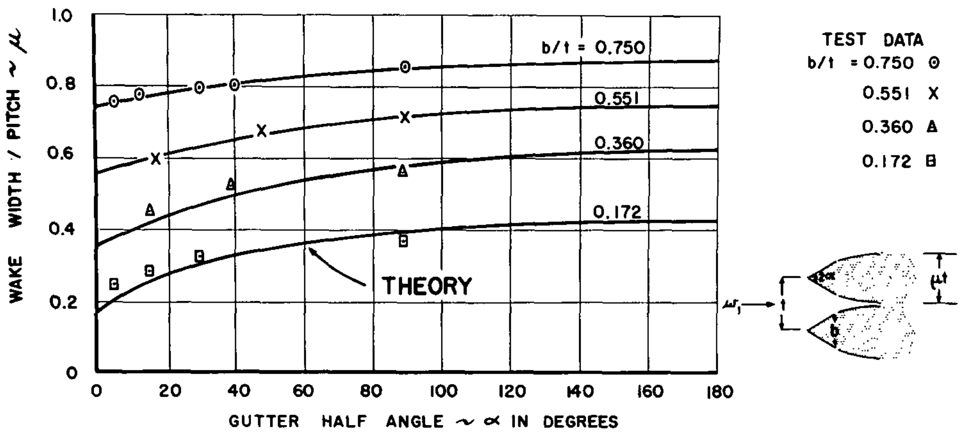

Fig. 11a - Comparison of theory and experiment for wake width to pitch ratio of vee-gutter cascade

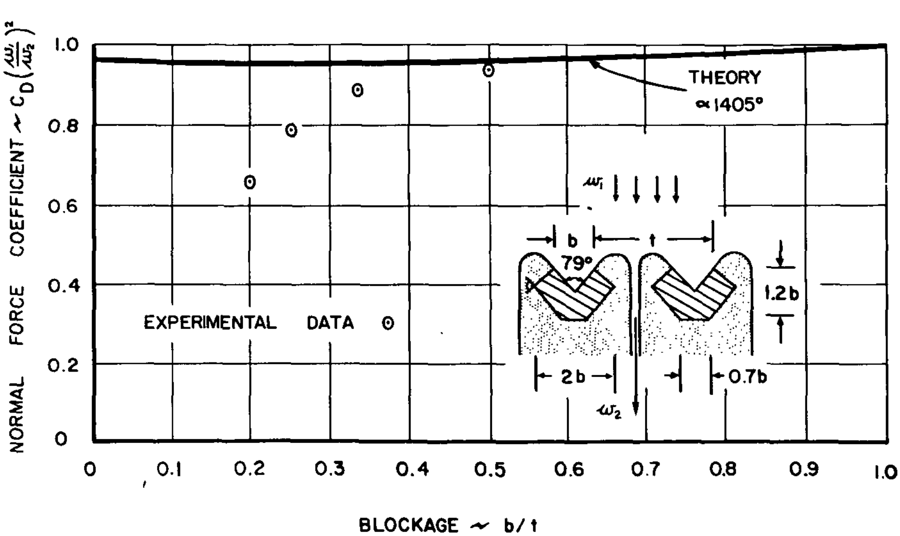

Fig. 11b - Comparison of theory and experiment for normal-force coefficient of vee-gutter cascade of 140.5° half-angle

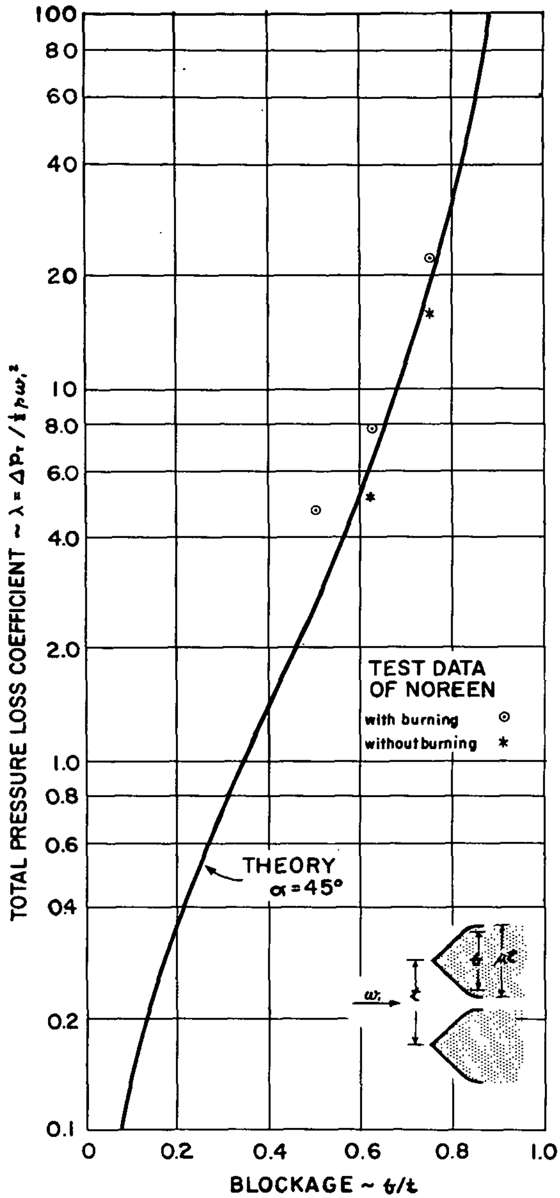

Fig. 11c - Comparison of theory and experiment for total-pressure loss coefficient of vee-gutter cascade of 45° half-angle

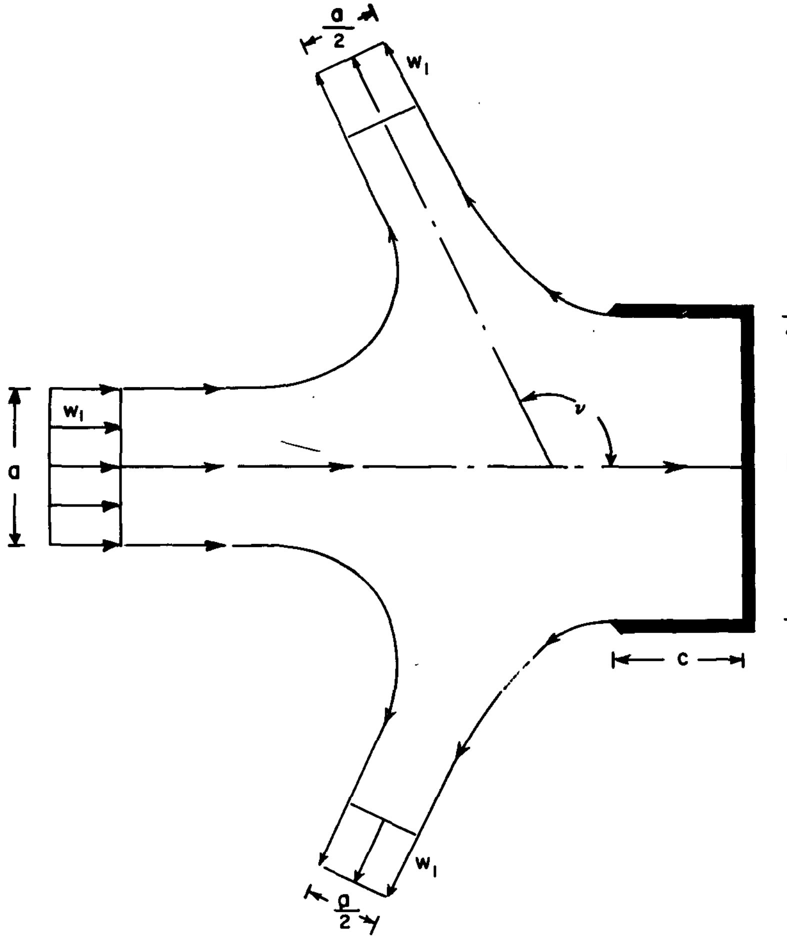

Fig. 12 - Model for flow over cylindrical thrust reverser

From the point of view of thrust reverser effectiveness, viz., largest deflection angle ν for smallest target size, the results of the two configurations show that thrust reversal ($\nu > 90°$) begins at $b/a = 2$, smaller targets giving $\nu < 90°$. Little additional deflection is obtained above about $b/a = 4$. For the cylindrical target, increasing axial length much above about $c/a = 1.5$ gives little additional deflection. For the conical target, the included half-angle $\pi - \alpha$, must be less than $90°$ in order to get reversal. As $\pi - \alpha$ is decreased from $90°$, deflection increases at a decreasing rate. Generally speaking, the conical target requires greater axial length than the cylindrical target, for the same diameter and deflection angle, making the latter preferable because of smaller size and weight.

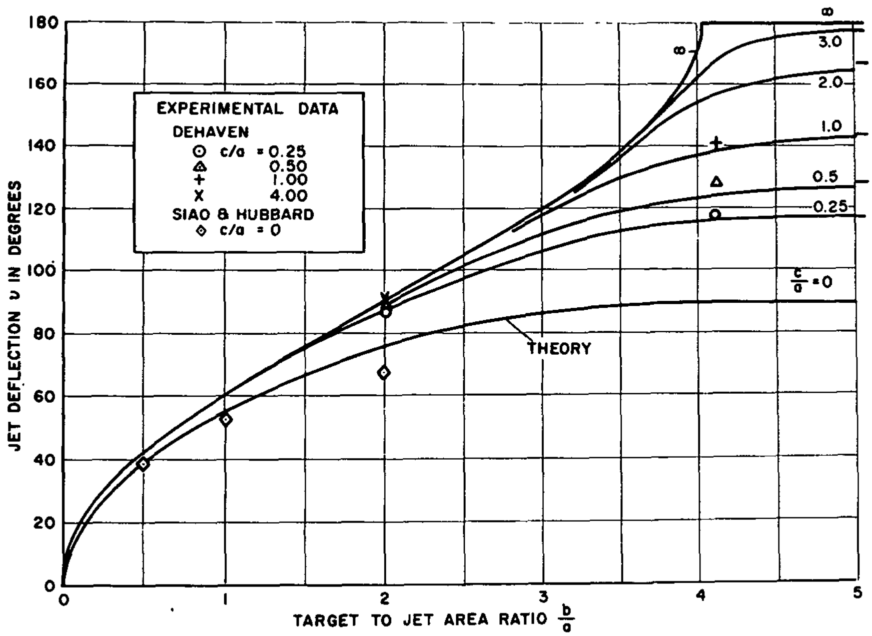

Fig. 13 - Comparison of theory and experiment for jet deflection angle of cylindrical thrust reverser

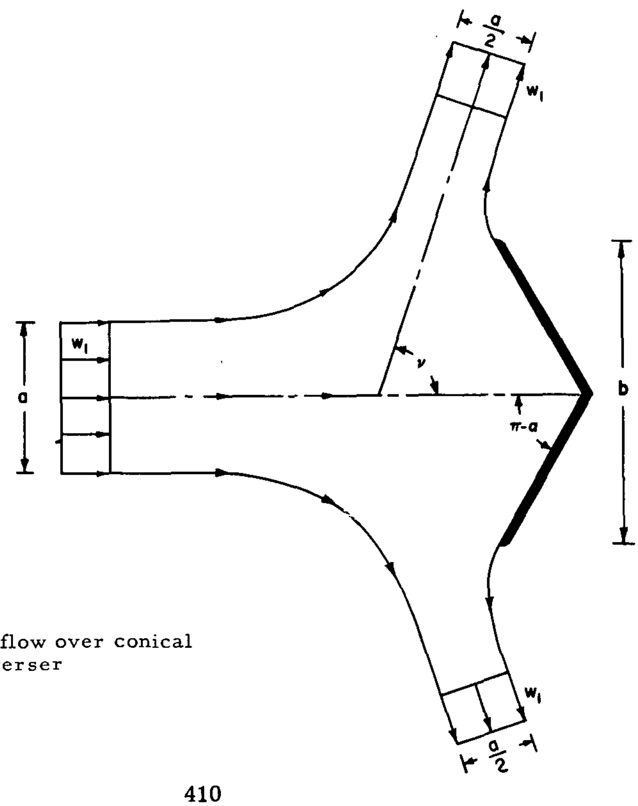

Fig. 14 - Model for flow over conical thrust reverser

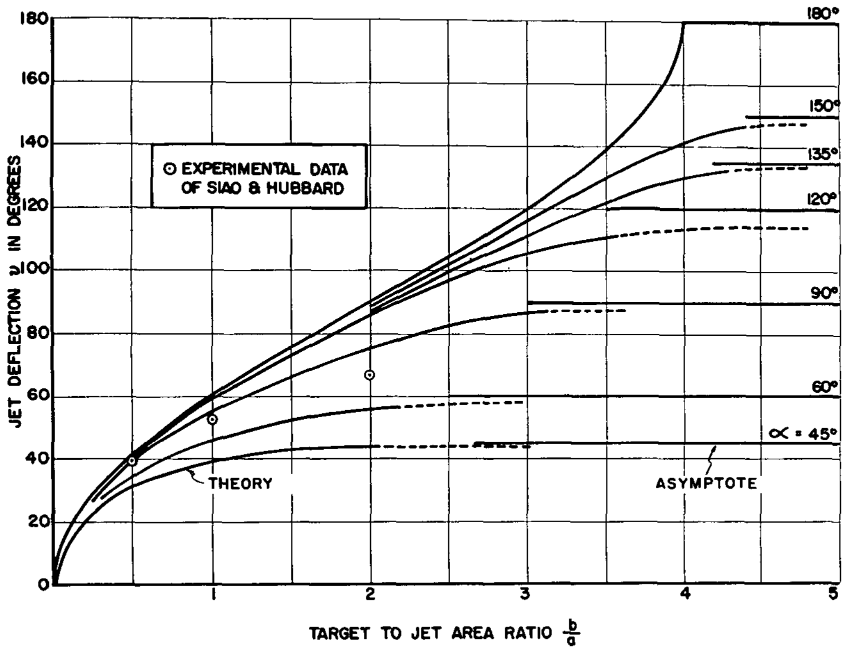

Fig. 15 - Comparison of theory and experiment for jet deflection angle of conical thrust reverser

THE BUTTERFLY VALVE

Butterfly or damper valves are frequently used as flow regulators in liquid rocket engine piping, aircraft gas turbine control system piping, and aerodynamic test facility ducting. It is desirable to predict the flow characteristics and total-pressure losses of such valves, as well as the forces acting on the regulating plates. A two-dimensional model of a butterfly valve is shown in Fig. 16. A plate of breadth t is placed in a channel of the same breadth making an angle α with the channel axis. Gaps of breadth $(1/2)e = (1/2)t(1 - \sin\alpha)$ exist at each side of the plate. A cavity is formed behind the plate, having breadth $t - (1/2)e(\varphi' + \varphi'')$ infinitely far downstream from the plate. The asymmetry of the configuration causes different breadths $\varphi' e/2$ and $\varphi'' e/2$ of the jets outside of the cavity. The velocity w_2 exists in both jets, assuming uniform static pressure at Section 2. The "average" contraction coefficient of the valve may be regarded as $(1/2)(\varphi' + \varphi'')$.

Ehrich (30) made an approximate analysis of the model configuration by treating the flow in two parts as shown in Fig. 17. The two approximate component configurations have unknown upstream breadths respectively equal to $t'/2$ and $t''/2$, where $t' + t'' = t$; otherwise boundary conditions are the same. Then, Ehrich recognized that the configurations of Fig. 17 were equivalent to von Mises' (26) two-dimensional contractions (or, likewise, the author's (25) vee-gutter cascades). Thus the contraction coefficients φ' and φ'' may be obtained as $\varphi'(s', \pi - \alpha)$ and $\varphi''(s'', \alpha)$, where $s' = 1 - e/t'$ and $s'' = 1 - e/t''$ are respectively the blocked area ratios of the two approximate configurations and $\pi - \alpha$ and α are the wall angles. Then, the contraction coefficient $(1/2)(\varphi' + \varphi'')$ is obtained in terms of valve closure angle α. Ehrich

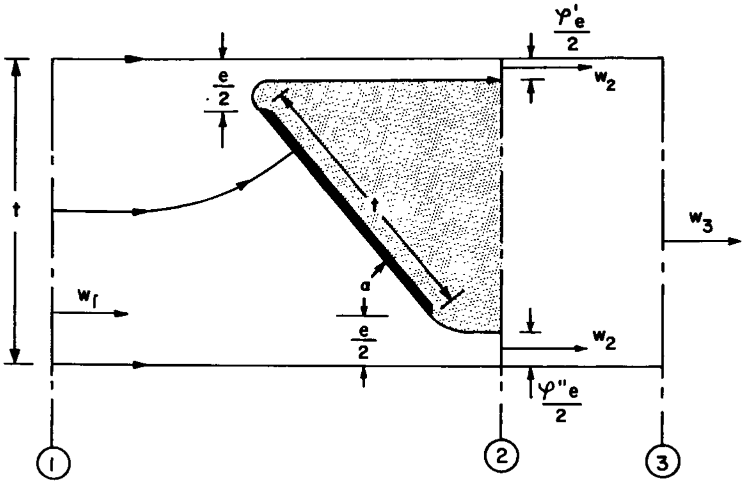

Fig. 16 - Model for flow in butterfly valve

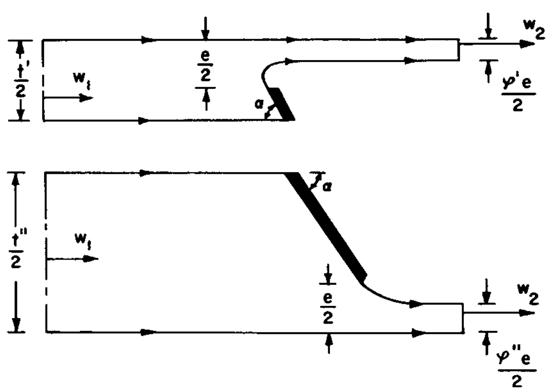

Fig. 17 - Approximate model for flow in butterfly valve

obtained the (normal) force acting on the valve plate by consideration of momentum and continuity, in terms of component axial and lateral force coefficients as:

$$C_{ax} = F_{ax}/(1/2)\rho w_1^2 t = \left\{[2t/e(\varphi' + \varphi'')] - 1\right\}^2 \tag{18a}$$

$$C_{lat} = F_{lat}/(1/2)\rho w_1^2 t = \left\{[2t/e(\varphi' + \varphi'')] - 1\right\}^2 \cot \alpha \tag{18b}$$

where $e/t = 1 - \sin \alpha$. Thus, the valve force is obtained as a function of valve closure α.

The total-pressure loss across the valve may be obtained by assuming complete mixing of the cavity and jets to yield a uniform flow of velocity $w_3 = w_1$ at Section 3 as shown in Fig. 16. Thus, from continuity and momentum considerations (as in the case of the slat cascade analysis), the total-pressure loss coefficient λ is given by

$$\lambda = (p_{T1} - p_{T3})/(1/2)\rho w_1^2 = \left\{[2t/e(\varphi' + \varphi'')] - 1\right\}^2 \tag{19}$$

which yields $\lambda(\alpha)$.

Figures 18a and 18b show the theoretical results of contraction coefficient φ and loss coefficient λ as functions of valve closure angle α. The theoretical loss coefficient λ is compared to three-dimensional test data of Weisbach (31), with the latter being largest, presumably because of the approximation introduced in the analysis (compare vee-gutter cascade results).

Other interesting valve configurations analyzed by Ehrich (30) include flapper, needle, orifice plate, gate, and spool valves.

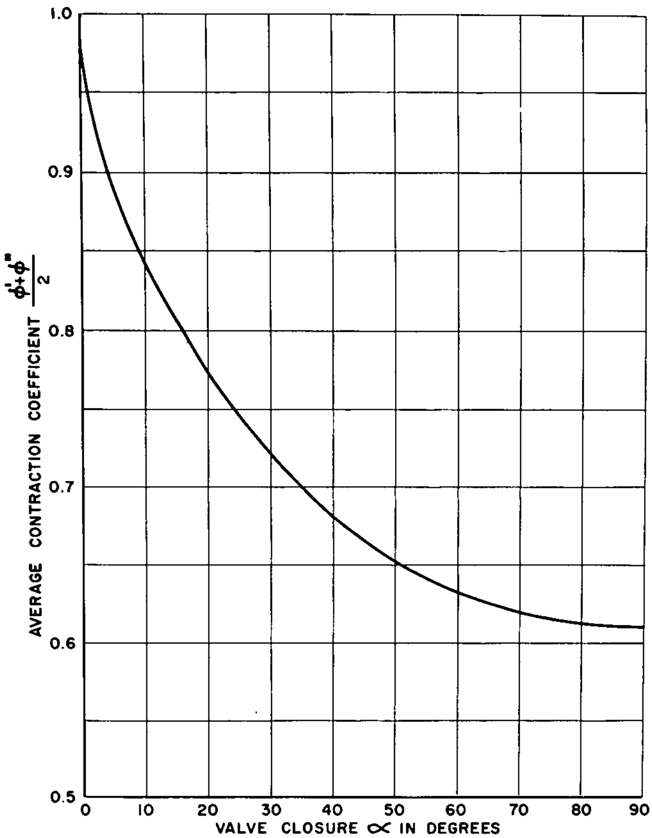

Fig. 18a - Theoretical average contraction coefficient of butterfly valve

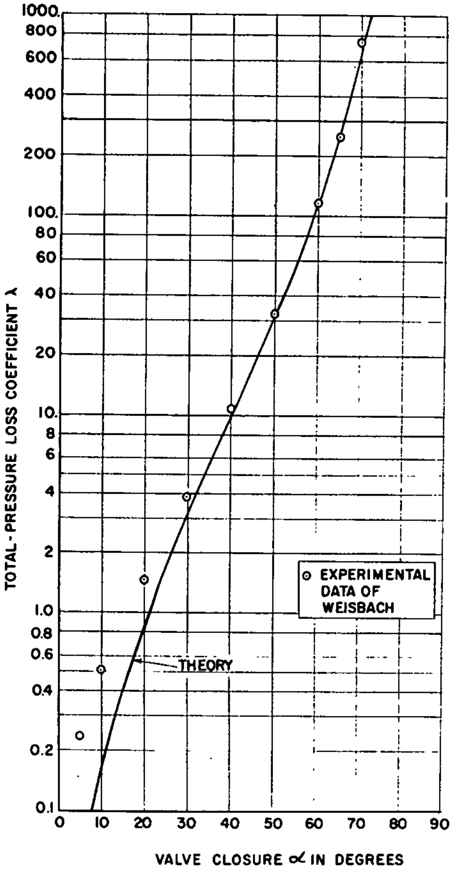

Fig. 18b - Comparison of theory and experiment for total-pressure loss coefficient of butterfly valve

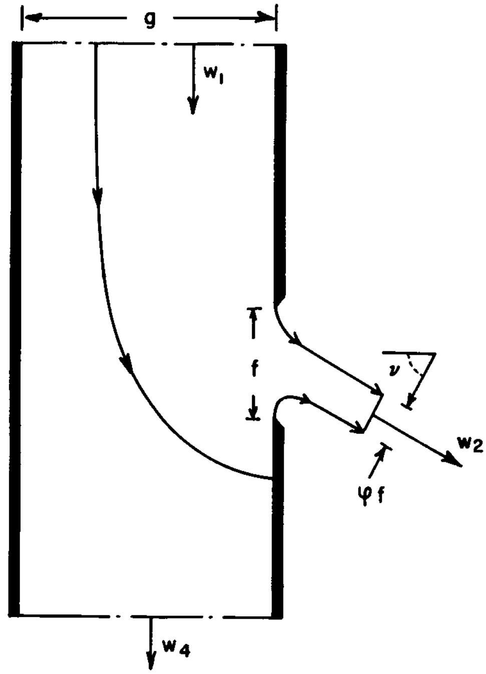

Fig. 19 - Model for flow in perforated combustor liner

THE PERFORATED COMBUSTOR LINER

In primary combustion systems for aircraft gas turbines the combustor configuration usually consists of one or more cylindrical containers, each having a concentric inner cylinder perforated with various holes, slots, and louvers. Air flowing axially in the annular space between the cylinders enters the inner cylinder through the perforations, is mixed with fuel, and burned, leaving downstream. Thus, there is considerable practical interest in the flow of air through a sharp-edged opening in a wall having air flow along it. It is desired to predict the flow through the opening and the "penetration" (described by flow angle) of the jet into the downstream space. McNown and Hsu (32) have studied the model shown in Fig. 19. A two-dimensional channel of breadth g has uniform velocity w_1 at infinity. A slot of breadth f in one wall forms a jet having area φf and velocity w_2 at infinity. The jet is deflected through an angle ν, relative to the upstream flow at Section 1. The remainder of the flow passes out of the channel with velocity w_4 at Section 4 at infinity. It is desired to predict the contraction coefficient φ and the jet deflection angle ν for various slot/channel breadth ratios f/g and various amounts of jet flow as characterized by the velocity ratio w_4/w_1. McNown and Hsu obtained the solution by the classical method. The theoretical results are shown in Fig. 20, where φ and ν are shown as functions of f/g and w_4/w_1.

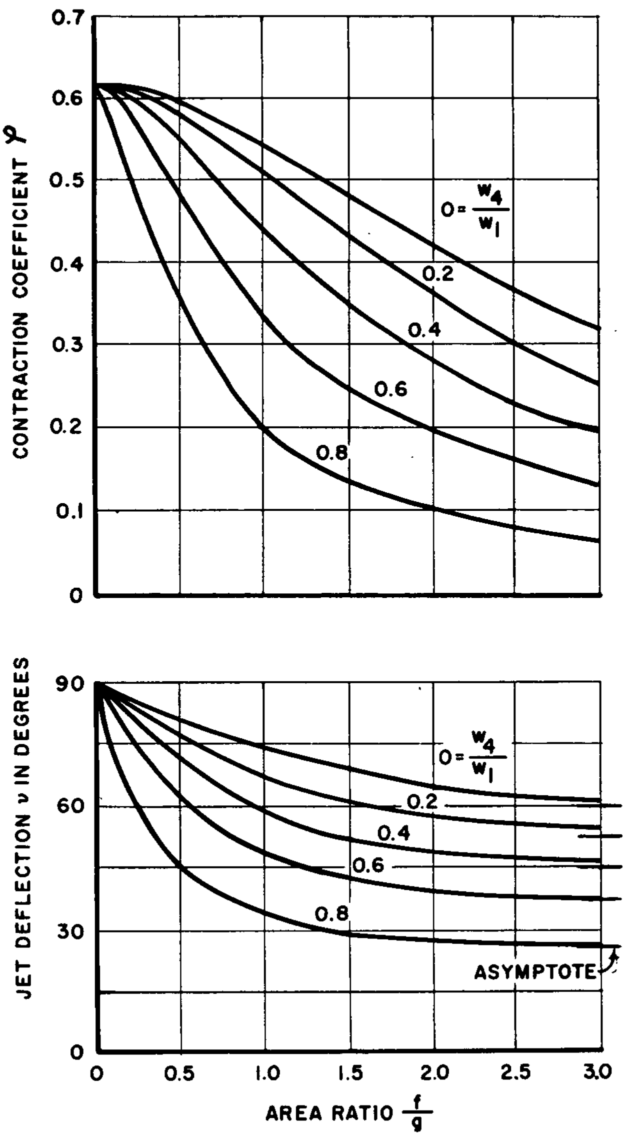

Fig. 20 - Theoretical contraction coefficient and jet deflection angle of perforated combustor liner

Ehrich (33) analyzed a different case having combustion interest, wherein air is fed through a sharp-edged slot into a parallel flow which is directed along the wall. For the case of equal total-pressures of the two streams, the surface of separation between the streams was calculated, as well as the free streamline separating the jet from the downstream solid boundary. Qualitative agreement was obtained between theoretical jet shapes and those obtained experimentally.

COMPRESSIBILITY EFFECTS IN AERODYNAMIC CAVITY FLOWS

The various solutions discussed above assume incompressible flow and yield reasonable results as long as this and the other assumptions are justifiable. However, in cases of high blockage or high inlet Mach number (ratio of flow velocity to velocity of sound) or both, results are a strong function of Mach number, since very high velocities then occur in the jets. In such cases, the compressibility effect is important. Analytical methods are not available for handling the general case. However, for specific configurations, solutions can be made in a manner entirely similar to the incompressible calculations.

An example of a compressible case is that of the slat cascade, treated by the author (24) in the study of flow through sharp-edged screens. In this case, the contraction coefficient φ was estimated as a function of blockage b/t and jet Mach number M_2. The estimation of φ was based on air test data on conical flow nozzles, taken over a range of nozzle pressure ratios. Then, compressible mixing calculations yielded the theoretical results shown in Fig. 21, where loss coefficient λ is shown as a function of inlet Mach number M_1 for various blockages $s = b/t$. The loss coefficient λ rises with M_1 for a given b/t, as might be physically expected. A subsonic flow limit curve is shown, the locus of conditions such that $M_2 = 1$. The curves are shown dashed beyond this limit because they are extrapolations, the one-dimensional mixing calculations used being invalid in this region. Further, additional shock wave losses will occur in supersonic jets. The curves are terminated by the envelope curve labeled "upper bound for choke," the locus of conditions such that sonic velocity exists across the entire opening of breadth $t - b$. Actual choking conditions will obtain somewhere between the subsonic flow limit and the upper bound for choke. Additional calculations could be made to yield compressible drag coefficients for the slat cascade.

A comparison of theoretical predictions of loss coefficient λ with experimental results (24) is shown in Fig. 22, for air tests of two perforated plates. Reasonable agreement is found between theory and test.

SCALE EFFECTS IN AERODYNAMIC CAVITY FLOWS

In cases where separation points are definitely fixed by the geometry (sharp edges) and where fluid-friction forces in the average streamwise direction acting on solid surfaces are negligible, e.g., the slat cascade, little scale effect is found (24). At very low Reynolds numbers (based on upstream velocity w_1 and slat breadth b) the loss coefficient λ may be expected to fall and then rise again as the Reynolds number is decreased, and likewise for the drag coefficient C_D. The contraction coefficient φ may be expected to rise and then fall again as the Reynolds number falls, similar to the case of the single sharp-edged orifice.

In cases where separation points are geometrically fixed, but fluid-friction forces in the average streamwise direction are not negligible, e.g., the vee-gutter cascade, some scale effect is to be expected. At low Reynolds numbers the loss coefficient λ may be expected to rise with falling Reynolds number, and likewise for the drag coefficient C_D. The contraction coefficient may be expected to fall with falling Reynolds number, similar to the case of the rounded flow nozzle.

In cases where the separation points are not geometrically fixed and fluid-friction forces in the average streamwise direction are not negligible, e.g., a cascade of cylinders, a large scale effect is to be expected. As in the case of the single circular cylinder, the locations of the separation points will vary with the Reynolds

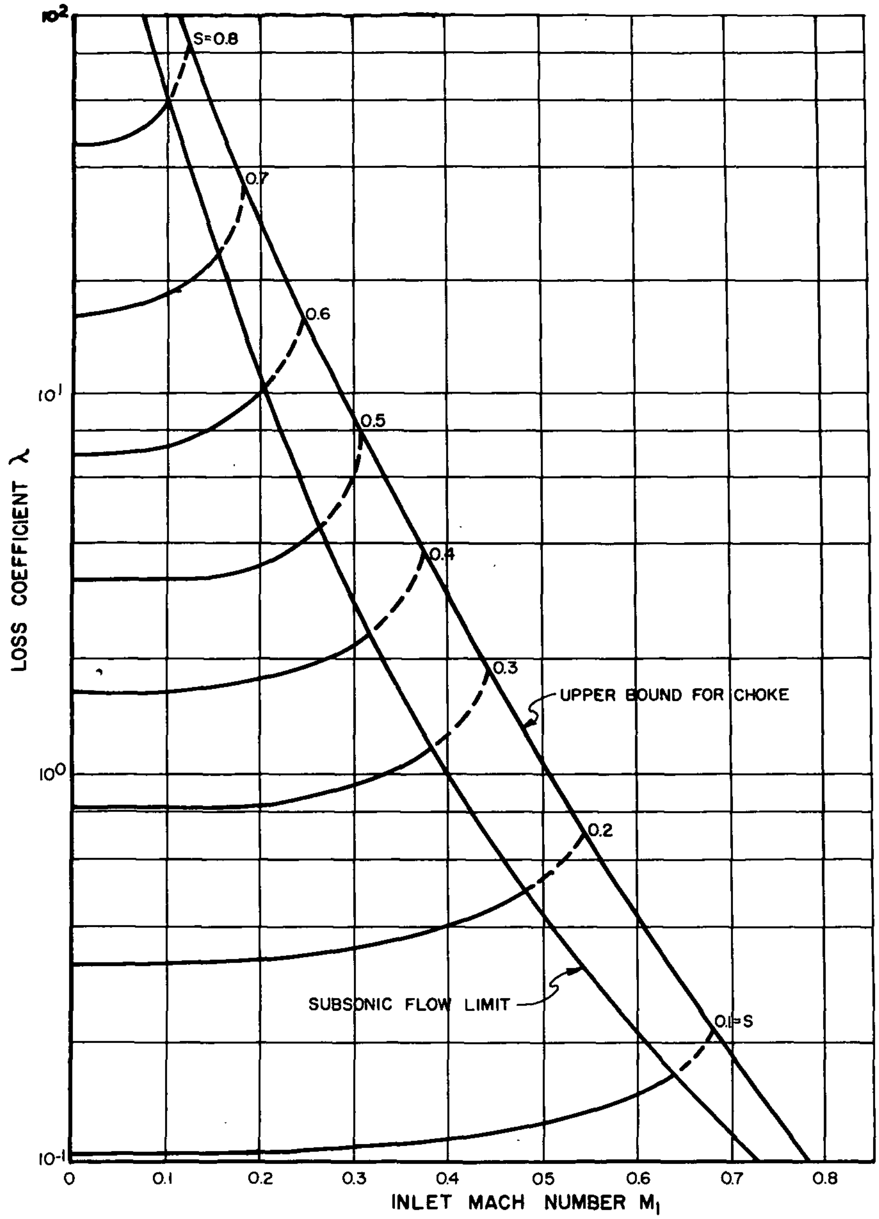

Fig. 21 - Theoretical compressible total-pressure loss coefficient of slat cascade or perforated plate

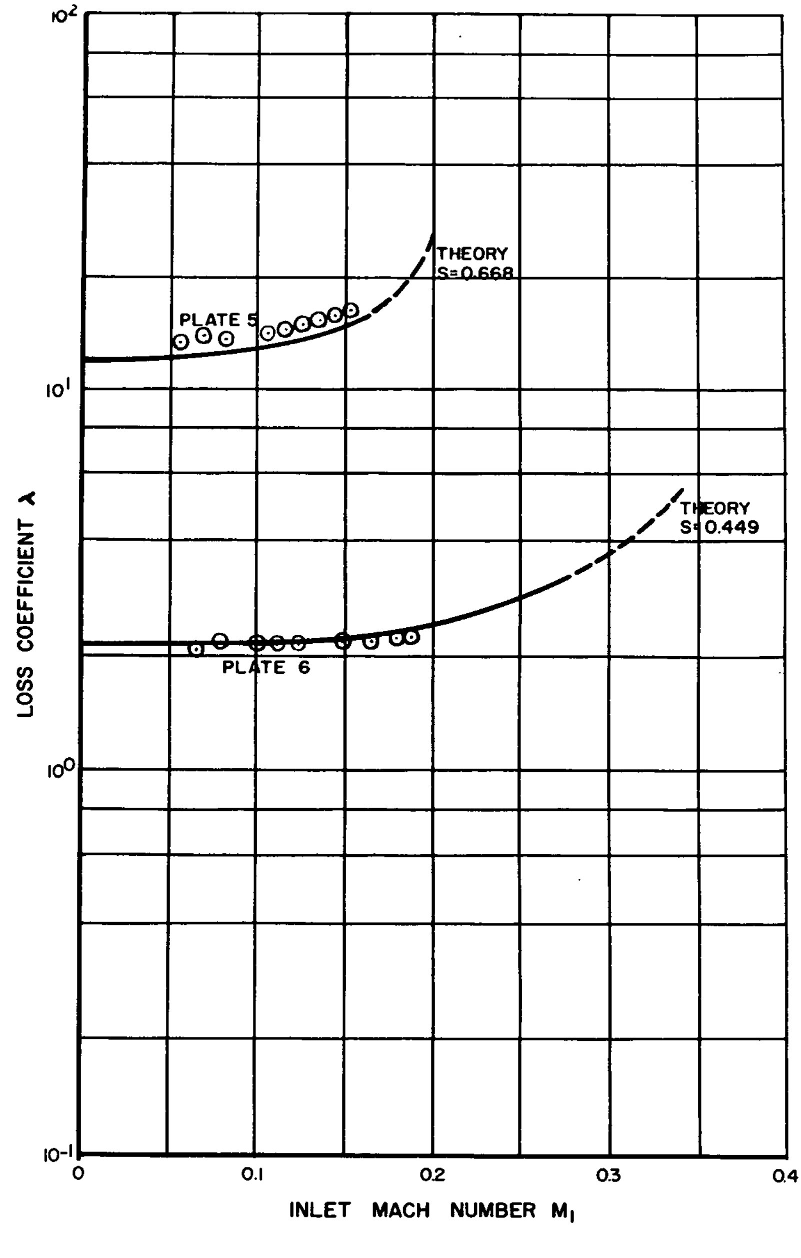

Fig. 22 - Comparison of theory and experiment for compressible total-pressure loss coefficient of perforated plates

number and, possibly, the entire character of the flow will likewise vary. For example, experimental data on round-wire screens (24) show a strong increase in drag coefficient C_D as the Reynolds number decreases in the region of low Reynolds numbers.

CONCLUSIONS

In aerodynamic cavity flows, viz., long cavities or wakes of relatively low velocity trailing behind solid obstacles in gas flows, reasonable results can be obtained in predicting cavity shape, drag force, and total-pressure loss by use of the free streamline method of Helmholtz-Kirchoff, along with mixing calculations, if the flow velocities, are low enough to justify the assumption of incompressible flow, solid surfaces can be approximated by linear elements, the Reynolds number is not too low, and jet velocities adjacent to the cavities are high enough to justify the assumption of a stagnant cavity.

Results can be obtained for higher velocity flows, if the effect of compressibility on cavity shape can be estimated analytically or otherwise. Scale effect (Reynolds number effect) will not be large in cases where the separation points (cavity inception) are fixed by sharp edges and where one may neglect the fluid-friction forces in the average streamwise direction on the solid surfaces. In other cases, the qualitative nature of the scale effect may be estimated.

ACKNOWLEDGMENT

The author is indebted to Mrs. Barbara Emmons for preparation of the present manuscript.

NOMENCLATURE

a = jet breadth upstream of thrust reverser (ft)

b = breadth of configuration element in direction transverse to upstream flow direction (ft)

c = axial depth of cylindrical thrust reverser (ft)

C_D = drag force coefficient, referred to upstream velocity head

C_L = lift force coefficient, referred to upstream velocity head

C_N = normal force coefficient, referred to upstream velocity head

D = drag force per unit span length (lb/ft)

e = opening of butterfly valve, measured normal to valve axis (ft)

f = breadth of bleed slot in wall of combustor liner (ft)

g = breadth of channel upstream of bleed slot in combustor liner (ft)

i = $\sqrt{-1}$

l = chord of flat plate cascade (ft)

L = lift force per unit span length (lb/ft)

H = $\ln \zeta$ = non-dimensional complex position variable in the logarithmic hodograph plane

M = Mach number

N = normal force per unit span length (lb/ft)

p = static pressure (lb/ft^2)

p_T = total-pressure (lb/ft^2)

s = blocked-area ratio of butterfly valve or perforated plate

t = pitch or spacing between configuration elements (ft)

u = x component of fluid velocity (ft/sec)

U = reference velocity (ft/sec)

v = y component of fluid velocity (ft/sec)

w = fluid velocity (ft/sec)

W = $\Phi + i\Psi$ = complex potential (ft^2/sec)

x = abscissa in the physical plane (ft)

y = ordinate in the physical plane (ft)

z = $x + iy$ = complex position variable in the physical plane (ft)

Z = complex position variable in the auxiliary half-plane (ft)

α = included half-angle of vee-gutter cascade or valve closure angle of butterfly valve or external half-angle of conical thrust reverser

β = fluid angle measured relative to normal to cascade axis

γ = stagger angle of flat plate cascade

δ = $\beta_1 - \gamma$ = angle of attack in flat plate cascade

Δp_T = $p_{T1} - p_{T3}$ = total-pressure loss (lb/ft^2)

ϵ = $\beta_1 - \beta_3$ = overall deflection angle of flat plate cascade

ζ = $(u - iv)/U$ = nondimensional complex position variable in the hodograph plane

θ = $\beta_1 - \beta_2$ = jet deflection angle of flat plate cascade

λ = $\Delta p_T/(1/2)\rho w_1^2$ = total-pressure loss coefficient, referred to upstream velocity head

Λ = w_1/w_2 = velocity ratio

μ = cavity breadth as a fraction of pitch t

ν = jet deflection angle of thrust reverser or combustor liner

φ = contraction coefficient (jet breadth as a function of configuration aperture breadth)

ρ = fluid mass density (slug/ft^3)

Φ = potential function (ft^2/sec)

Ψ = stream function (ft^2/sec)

Subscripts

ax = subscript referring to axial force in butterfly valve analysis

lat = subscript referring to lateral force in butterfly valve analysis

1 = subscript referring to conditions infinitely far upstream of configuration

2 = subscript referring to conditions infinitely far downstream of configuration

3 = subscript referring to conditions after mixing of jets and cavities

4 = subscript referring to conditions downstream of bleed slot in combustor liner

∞ = subscript referring to vector mean velocity in flat plate cascade

REFERENCES

1. Helmholtz, H., "Ueber diskontinuierliche Fluessigkeitsbewegungen," Monatsberichte Akademie der Wissenschaften, Berlin, 1868, pp. 215-228; also, Philosophical Magazine, November 1868

2. Kirchoff, G., "Zur Theorie freier Fluessigkeitsstrahlen," Crelle's, Journal fuer Mathematik 70:289-298 (1869)

3. Michell, J.H., "On the Theory of Free Streamlines," Philosophical Transactions of the Royal Society (London) A181:389-431 (1890)

4. Trefftz, E., "Ueber die Kontraktion kreisfoermiger Fluessigkeitsstrahlen," Zeitschrift fuer Mathematik und Physik 64:34-61 (1916); also, Dissertation, Strassburg, 1913

5. Flachsbart, O., "Messungen an ebenen und gewoelbten Platten," Ergebnisse der Aerodynamischen Versuchsanstalt zu Goettingen, IV Lieferung, 1932, pp. 96-100.

6. Riabouchinsky, D., Proceedings of the London Mathematical Society 19:206-215 (1921)

7. Gilbarg, D., and Rock, D.H., Naval Ordnance Laboratory Memorandum No. 8718, 1945

8. Roshko, A., "A New Hodograph for Free-Streamline Theory," National Advisory Committee for Aeronautics Technical Note 3168, July 1954

9. Weinig, F.S., "Computation of Drag in Separated Flow by Use of Rolling Up Free Streamlines," Proceedings of the 9th International Congress for Applied Mechanics, Brussels, 1957, Vol. 1, pp. 215-220

10. Tulin, M.P., "Steady Two-Dimensional Cavity Flows about Slender Bodies," David Taylor Model Basin Report 834, May 1952

11. McNown, J.S., "Elements of Free-Streamline Theory," in "Free-Streamline Analyses of Transition Flow and Jet Deflection," State University of Iowa, Studies in Engineering, Bulletin 34, 1953, pp. 3-14

12. Birkhoff, G., "Hydrodynamics - A Study in Logic, Fact and Similitude," Princeton University Press, 1950, pp. 40-76

13. Planck, M., "Zur Theorie der Fluessigkeitsstrahlen," Annalen der Physik und Chemie 21:499-509 (1884)

14. Christoffel, E.B., "Sul Problema delle Temperature Stazionarie e la rappresentazione di una Data Superficie," Annali di Matematica, Series 2, 1:95-103 (1867)

15. Schwarz, H.A., "Notizia sulla rappresentazione conforme di un'area ellittica sopra un'area circolare," Annali di Matematica, Series 2, 3:166 (1869)

16. Lord Rayleigh, "Notes on Hydrodynamics," Philosophical Magazine, December 1876

17. Lamb, H., "Hydrodynamics," 6th ed., New York:Dover (reprint) 1945

18. Milne-Thomson, L.M., "Theoretical Hydrodynamics," 2nd ed., New York:MacMillan, 1950

19. Cornell, W.G., "The Stall Performance of Cascades," Proceedings of the Second U.S. National Congress of Applied Mechanics, Ann Arbor, Michigan, 1954, pp. 705-713

20. Betz, A., and Petersohn, E., "Anwendung der Theorie der freien Strahlen," Ingenieur-Archiv 2:190-211 (1931); see also National Advisory Committee for Aeronautics Technical Memorandum 667, 1932

21. Weisbach, J., "Die Experimental-Hydraulik," Freiberg:Engelhardt, 1855

22. Grey, R.E., and Wilsted, H.D., "Performance of Conical Jet Nozzles in Terms of Flow and Velocity Coefficients," National Advisory Committee for Aeronautics Technical Note 1757, November 1948

23. Langer, R., "Bremswirkung von Windschutzgittern," Ergebnisse der Aerodynamischen Versuchsanstalt zu Goettingen, IV Lieferung, 1932, pp. 138-141

24. Cornell, W.G., "Losses in Flow Normal to Plane Screens," Transactions of the American Society of Mechanical Engineers 80(No. 4):791-799 (1958)

25. Cornell, W.G., "The Flow in a Vee-Gutter Cascade," Transactions of the American Society of Mechanical Engineers 78(No. 3):573-580 (1956)

26. von Mises, R., "Berechnung von Ausfluss- und Ueberfallzahlen," Zeitschrift des Vereines deutscher Ingenieure 61(No. 21):447-452 (1917); 61(No. 2):469-474 (1917); and 61(No. 23):493-498 (1917)

27. Noreen, A.E., unpublished, 1954

28. Sarpkaya, T., "Deflection of Jets - Symmetrically Placed U-Shaped Obstacles," in "Free-Streamline Analysis of Transition Flow and Jet Deflection," State University of Iowa, Studies in Engineering, Bulletin 35, 1953, pp. 45-53

29. Siao, T-T, and Hubbard, P.G., "Deflection of Jets - Symmetrically Placed V-Shaped Obstacles," in "Free-Streamline Analysis of Transition Flow and Jet Deflection," State University of Iowa, Studies in Engineering, Bulletin 35, 1953, pp. 33-34

30. Ehrich, F.F., "Some Hydrodynamic Aspects of Valves," American Society of Mechanical Engineers, Paper No. 55-A-114, November 1955

31. Merriman, M., "Treatise on Hydraulics," 8th ed., New York:Wiley, 1907, pp. 216-217

32. McNown, J.S., and Hsu, E-Y, "Application of Conformal Mapping to Divided Flow," Proceedings of the First Midwestern Conference on Fluid Dynamics, May, 1950, Ann Arbor:Edwards, 1951, pp. 143-155

33. Ehrich, F.F., "Penetration and Deflection of Jets Oblique to a General Stream," Journal of the Aeronautical Sciences 20:99-104 (1953)

* * * * *

DISCUSSION

G. Birkhoff (Harvard University)

This is an excellent review of the favorable side of the ledger, as regards predictions of real wake behavior from mathematical solutions of the Helmholtz Problem. Perhaps in Dr. Cornell's discussion of general conformal mapping methods more emphasis might have been put on the parameter problem: in most cases, the greatest difficulty comes in determining the auxiliary constants (parameters) of the Schwarz-Christoffel transformations involved.

I was unable to understand clearly the "constant momentum mixing" hypothesis used, and wonder if it is mathematically equivalent to the following naive method of calculation. Let two parallel streams of equal density ρ, thicknesses τ_1, τ_2, and velocities v_1, v_2, mix as they flow downstream under Helmholtz instability. The mean downstream velocity, $v_o = (T_1v_1 + T_2v_2)/(T_1 + T_2)$, should be regarded as zero relative to this, by the Bernoulli equation

$$p_1 + 1/2\ \rho(v_1 - v_o)^2 = p_2 + 1/2\ \rho(v_2 - v_o)^2 .$$

In 1943, I suggested this method of calculation to the late John von Neumann as a basis for calculating wake underpressure (in this case, $T_2 = \infty$ and $v_o = v_2$). He pointed out that for most cases (though not for a broadside flat plate) it seriously over-estimated the wake underpressure.

M. Tulin (Office of Naval Research)

Has there been any application of cavity-flow models to the prediction of flameout?

W. G. Cornell

With respect to flameout, I would say no. So far, most applications have been to predict so-called dry losses in the flameholders which are put in to stabilize combustion.

* * * * *